Progress In Electromagnetics Research C, Vol. 19, 119–133, 2011

DEVELOPMENT OF CIRCULARLY POLARIZED ARRAY ANTENNA FOR SYNTHETIC APERTURE RADAR SENSOR INSTALLED ON UAV

Yohandri, V. Wissan, I. Firmansyah, P. Rizki Akbar J. T. Sri Sumantyo and H. Kuze †

Microwave Remote Sensing Laboratory
Center for Environmental Remote Sensing, Chiba University
1-33, Yayoi-cho, Inage-ku, Chiba 263-8522, Japan

Abstract—We have developed an array antenna consisting of 12 elements of simple square-shaped, corner-truncated patches for circularly polarized synthetic aperture radar (CP-SAR) operated in the L-band. The corporate feed design concept is implemented by combining a split-T and a 3-way circular-sector-shape power divider to excite circularly polarized radiation. The fabricated antenna based on the simulation using moment method gives a good circular polarization at the center frequency of 1.27 GHz with an impedance bandwidth of 6.1% and 3-dB axial ratio bandwidth of 1.0%, satisfying the specification for our circularly polarized synthetic aperture radar intended for use onboard an unmanned aerial vehicle and a small satellite.

1. INTRODUCTION

When propagating in the ionosphere, linearly polarized microwave is disturbed by the Faraday rotation effect caused by the interaction with electrons and magnetic fields [1, 2]. Depending on the viewing angle and the solar cycle [3], the resulting rotation of electric field vectors can be as much as a few tens of degrees, degrading the performance of L-band microwave remote sensing for targets such as soil moisture and sea surface salinity.

The effect of Faraday rotation can be reduced by transmitting the microwave in circular polarization (CP) [4]. The quality of CP

Received 17 December 2010, Accepted 7 January 2011, Scheduled 18 January 2011
Corresponding author: Yohandri (yohandri@graduate.chiba-u.jp).
† Yohandri is also with Physics Department, State University of Padang, Kampus UNP Jln. Prof. Hamka Air Tawar, Padang, West Sumatera 25131, Indonesia.

signals can be described by a parameter called axial ratio (AR), the value of which is defined as the ratio of the major axis to the minor axis of the polarization ellipse, commonly given in dB unit. In addition, the direction of polarization can be classified into two types, namely left-handed (LH) and right-handed (RH), indicating the sense of rotation of the wave front. Currently synthetic aperture radar (SAR) sensor based on CP (CP-SAR) is developed in the Microwave Remote Sensing Laboratory (MRSL), Center for Environmental Remote Sensing (CEReS), Chiba University [5]. This sensor is operated in the L-band, and will be mounted onboard a small satellite (μSAT), as illustrated in Figure 1. This μSAT will be equipped with RHCP and LHCP array antennas and a GPS radio occultation sensor, as well as a solar array panel. This sensor is intended for several applications such as land cover and snow cover mapping, oceanography mapping, and disaster monitoring. The capabilities of this novel CP-SAR sensor will be tested by mounting it onboard an unmanned aerial vehicle (UAV). The microwave signal from UAV platform is transmitted by LHCP or RHCP array antenna. The backscattering signal from the target is captured by both the LHCP and RHCP array antennas to generate the axial ratio image (see Figure 2(a)). To realize the high quality and efficiency in these applications, the CP-SAR parameters including size, weight, power consumption, etc. should be thoroughly considered. These parameters are related also to the aerodynamic stability of the UAV system. The design and photograph of UAV fabrication are shown in Figures 2(b) and 2(c), respectively.

The purpose of the present paper is to describe the development of the LHCP sub array microstrip antenna installed on UAV. In general, a microstrip antenna can attain a narrow frequency bandwidth

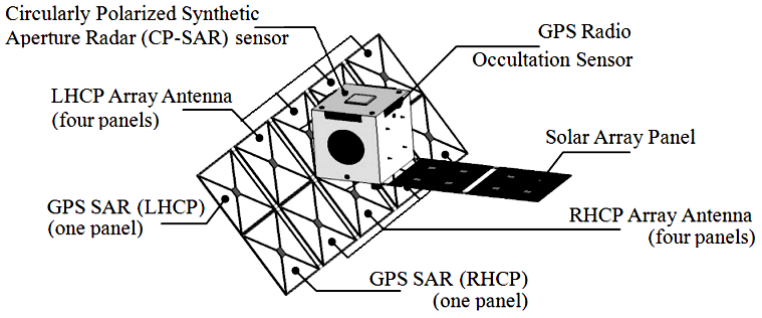

Figure 1. Circularly polarized synthetic aperture radar (CP-SAR) sensor onboard a small satellite (μSAT).

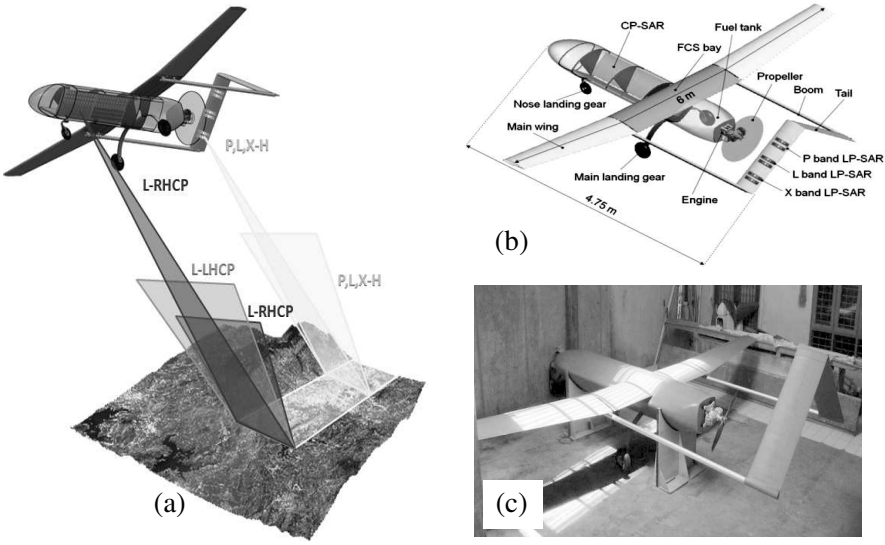

Figure 2. CP-SAR onboard an unmanned aerial vehicle (UAV), (a) transmitting and receiving system of signals, (b) design of UAV, and (c) photograph of UAV fabrication.

at the expense of a low gain. As compared with conventional microwave antennas, a microstrip antenna has additional advantages such as a compact size, light weight, conformability to surfaces of substrates, low cost, and easier integration with other circuits and versatility [6]. In previous works, several single element CP antennas have been fabricated in MRSL [7–9]. For CP-SAR applications, an array configuration must be adopted to satisfy the requirement of the system. Here we propose an L-band CP-SAR antenna consisting of 12 elements of simple square-shaped, corner-truncated microstrip antenna with a novel feeding network. A similar square-shaped CP array antenna has been reported [10] with a feed network using a T junction power divider. Obviously the limitation of this previous antenna design is that the possible power split must be 2^n $(n = 1, 2, 3 \ldots)$. In the present work, we propose the use of a circular sector power divider, which enables odd-number feeding as well. The proximity-coupled feeding method is adopted for feeding each patch element. The main advantage of this feed technique is the ease in both design and fabrication adjustment processes, resulting in good AR and impedance matching [11]. While a good AR is generally attained by controlling the feed point, the impedance matching can be achieved by controlling the length and width of the microstrip line.

Table 1. Essential antenna parameters for CP-SAR system.

Parameters	Specification	
	UAV	**μSAT**
Frequency center (GHz)	1.27	1.27
Pulse Bandwidth (MHz)	233.31	10
Axial ratio (dB)	≤ 3	≤ 3
Antenna efficiency	$> 80\%$	$> 80\%$
Antenna gain (dBic)	14.32	36.6
Azimuth beamwidth	$\geq 6.77°$	$\geq 1.08°$
Elevation beamwidth	$3.57° - 31.02°$	$\geq 2.16°$
Antenna size (m)	1.5×0.4	2×4
Polarization (Tx/Rx)	RHCP + LHCP	RHCP + LHCP

2. ARRAY ANTENNA DESIGN

2.1. Design Consideration

The excellent performance of the overall CP-SAR system can only be attained through optimizing the antenna design in terms of various antenna parameters such as the gain, directivity, AR, reflection coefficient, etc. Table 1 shows the essential parameters and specification of CP-SAR sensor onboard UAV [12] and μSAT [13].

In this research, the operating frequency of array antenna is fixed at 1.27 GHz (L-Band). Both a transmitter (Tx) and a receiver (Rx) are considered for both RHCP and LHCP operations, where the AR should be less than 3-dB within the targeted beamwidth to guarantee the radiation is circular polarization. Conversely, for the AR > 3-dB, the microwave polarization will be elliptical. The size of antenna proposed in Table 1 is for the combination of four sub-array panels, for each RHCP and LHCP.

2.2. Square Patch Antenna

The square patch geometry is chosen since it can easily be arranged and fabricated to produce CP radiation. For the sake of feeding, two opposite corners of each patch is truncated for either LHCP or RHCP operation. The first step in the design is to specify the dimension of a single element microstrip antenna. In practice, the patch dimension must be slightly less than a half wavelength ($23.6/2 = 11.8$ cm), in order to take fringing fields into consideration. The fringing fields along

the width can be modeled as radiating slots, and electrically the width of the microstrip antenna looks greater than its physical dimensions. Thus, the relation between the physical length, L, and the effective length, L_{eff}, can be written as [14]

$$L_{eff} = L + \Delta L, \tag{1}$$

where ΔL (length extension) stands for the effect of the fringe fields. For a given resonance frequency f_0, the effective length can be calculated as

$$L_{eff} = \frac{c}{2f_0\sqrt{\varepsilon_{eff}}}. \tag{2}$$

Here, c and ε_{eff} are the speed of light and effective dielectric constant, respectively. Empirically the value of ΔL is given as [15]

$$\Delta L = 0.412h\frac{(\varepsilon_{eff}+0.3)\left(\frac{h}{W}+0.262\right)}{(\varepsilon_{eff}-0.258)\left(\frac{h}{W}+0.813\right)}, \tag{3}$$

where W is the width of the microstrip patch and h is the substrate thickness: besides, ε_{eff} is given as

$$\varepsilon_{eff} = \frac{\varepsilon_r+1}{2} + \frac{\varepsilon_r-1}{2}\left[1+12\frac{h}{W}\right]^{-\frac{1}{2}}, \tag{4}$$

where ε_r is the dielectric constant of the substrate.

In this work, we have employed a substrate (NPC-H220A, Nippon Pillar Packing) having a thickness 3.2 mm, a dielectric constant $\varepsilon_r = 2.17$ and a loss tangent $\delta = 0.0005$. By entering the width of patch $W = 93.82$ mm and resonance frequency $f_0 = 1.27$ GHz, the effective length (L_{eff}) and effective dielectric constant (ε_{eff}) can be obtained 77.18 mm and 2.08, respectively.

2.3. Feeding Network Design

The basic components of the present antenna array are corner-truncated square patches, a split-T and a 3-way circular-sector-shaped power divider (Figure 3). The array is composed of three blocks, each of which consists of 2×2 patches (Figure 4). The circular-sector divider is used to divide the feed energy into the three blocks, and a split-T power divider is employed to divide the power equally into two parts at each division point. The optimal performance of the circular-sector divider can be achieved when the sector angle, α, is equal to 90° or 180° [16]. The power from a 50 Ω feed line is divided

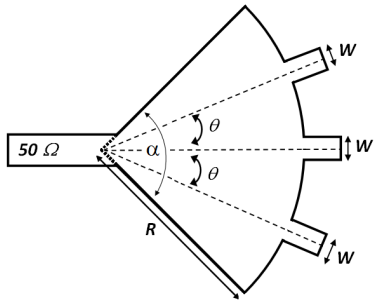

Figure 3. The 3-way circular-sector-shaped power divider.

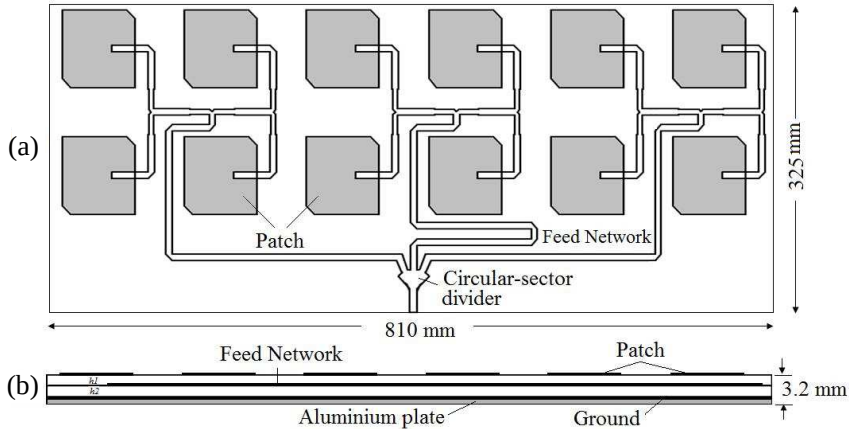

Figure 4. Configuration of the antenna array consisting of three blocks, each block having 2×2 element patches, (a) top view, and (b) side view.

symmetrically in the sector by placing each feed at an angular distance of $\theta = 22.5°$, with a width (W) of the feed of 6.8 mm and radius (R) of the circular-sector of 24 mm. Proposed antenna geometry with thickness $h_1 = h_2 = 1.6$ mm and a photograph of fabricated feed network is shown in Figure 4 and Figure 5.

The geometrical design of the antenna array is optimized using method of moment (the IE3D simulation software) by assuming a finite ground plane model. By adjusting several parameters indicated in Figure 6, the optimum parameters are obtained as listed in Table 2.

In Table 2, L_{ground} and W_{ground} are the total length and width of the ground plate. These dimensions (810 mm $\times$ 325 mm) are equal to the size of the fabricated antenna as shown in Figure 7.

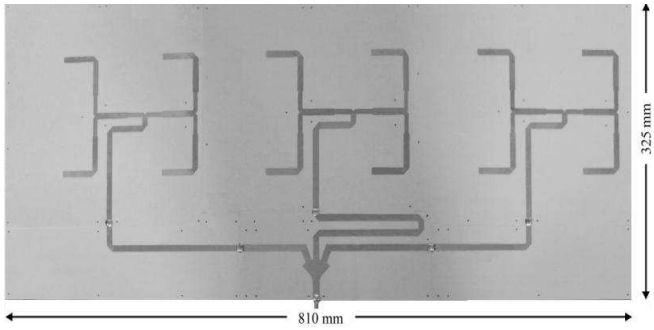

Figure 5. Photograph of the fabricated feed network (top view).

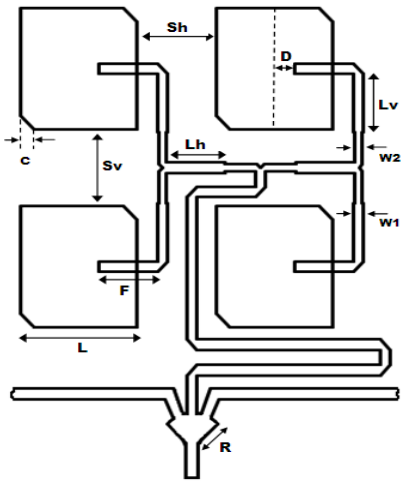

Figure 6. Geometry layout of a single piece of antenna array.

Parameters	Size (mm)
L	79.18
C	9.00
D	14.00
F, Lh	40.00
Lv	38.00
Sh	54.00
Sv	50.00
R	24.00
W_1	6.80
W_2	5.00
L_{ground}	810.00
W_{ground}	325.00

Table 2. Geometry parameters (mm) of circularly polarized array antenna.

3. ANTENNA CHARACTERISTICS

To realize the antenna characteristics similar to the simulation results, careful and precise fabrication process is indispensable. A high precision milling machine (Seven Mini) is used for the fabrication process that involves several steps such as milling, drilling and edge cutting. The etching technique is also implemented to remove unnecessary copper part of the microstrip substrate. A photograph of the fabricated array antenna is shown in Figure 7. A 2-mm thick aluminum plate is used to support the substrate. The length and width of the fabricated antenna are 810 mm and 325 mm, respectively. Total

weight of this sub antenna array is around 2.47 kg, within the tolerance of the UAV total payload (25 kg).

The antenna characteristics are measured using a RF Vector Network Analyzer (Agilent VNA E8364C). The antenna parameters are measured inside the anechoic chamber at MRSL. This chamber is equipped with a turntable with the controller, two conical log-spirals, LHCP/RHCP antennas and a dipole antenna as a standard reference. The schematic of the measurement system and the picture of AUT are shown in Figure 8.

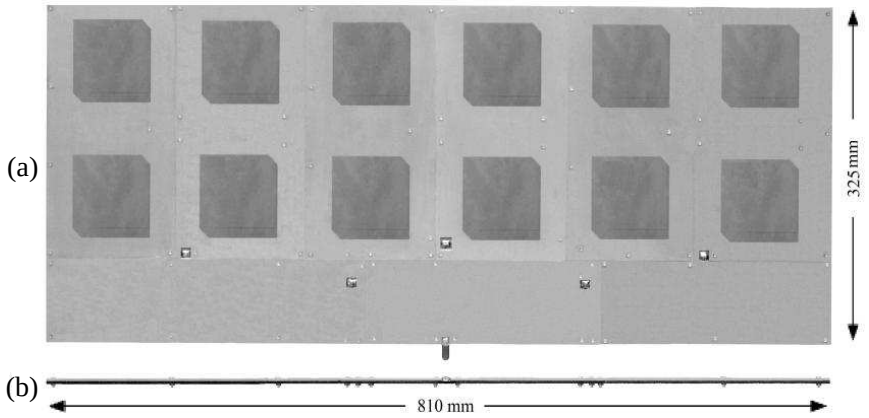

Figure 7. Photograph of the fabricated antenna array, (a) top view, (b) and side view.

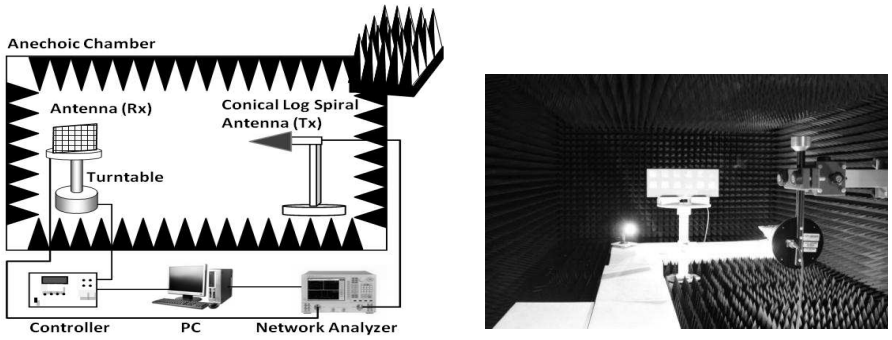

Figure 8. Measurement of antenna characteristics, (a) schematic of the measurement system and (b) a photograph of antenna under test in the MRSL anechoic chamber.

The AUT is mounted on a turntable, which is rotated using a precise positioning system that enables the precise alignment between AUT and the conical log-spiral antenna. Direction and speed of the turntable can be remotely controlled from outside of the chamber. The antenna characteristics measured by recording the power from the AUT at each position will be described in the following section.

4. RESULTS AND DISCUSSION

Figures 9–15 show the comparison between the measured and simulated results of the reflection coefficient (S_{11}), real input impedance (Z_{in}), axial ratio (AR), Gain (G) and radiation pattern. Figure 9 shows the frequency dependence of S_{11} measured for the fabricated antenna. The simulated and measured curves show similar behavior, exhibiting reflection minimum around 1.270–1.275 GHz, though somewhat higher resonance frequency is seen for the measurement. A slight difference of the working frequency between the simulation and measurement is presumably due to the effect of alignment errors in the fabrication of the antenna in the antenna range measurements and the effect of ground plane size. The difference in the minimum values of the reflection coefficient (-60 vs. -30 dB) can also be considered to the degradation during the fabrication process. Nevertheless, the measured value of the 10-dB impedance bandwidth is 77 MHz, approximately 6.1% of the resonance frequency of 1.275 GHz. This result is by 14 MHz wider than the simulated value of 63 MHz (5.0%). This dissimilarity result is probably attributed by the difference in the patch geometry and feed line size (between simulated and fabricated model) due to the substrate variation.

In Figure 10, the real input impedance is plotted against the frequency. The measured value at the working frequency of 1.27 GHz is 48.07 Ω, about 3.9% smaller than the simulated value of 50 Ω. In Figures 9 and 10, slight differences between the simulated and measured results are presumably due to the resistivity offering from milling process, a connector and soldering. In the feed network, the length of each element from the patch to connector must be fixed at $n\lambda/4$ ($n = 1, 3, 5, \ldots$) to achieve the optimal current intensity. The deviation of the length from the designed value can also contribute to the difference between the simulation and measurement.

The relation between the AR and frequency is plotted in Figure 11, showing the polarization characteristics of the fabricated antenna. The 3-dB AR bandwidth achieved at the direction of $\theta = 0^\circ$ (i.e., the AUT is set perpendicular to the standard antenna) is about 13 MHz, which corresponds to 1.02% of the operation frequency of 1.27 GHz.

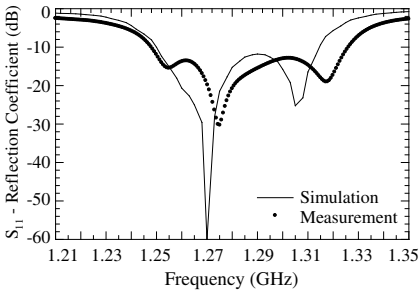

Figure 9. Simulated and measured reflection coefficient plotted as a function of frequency.

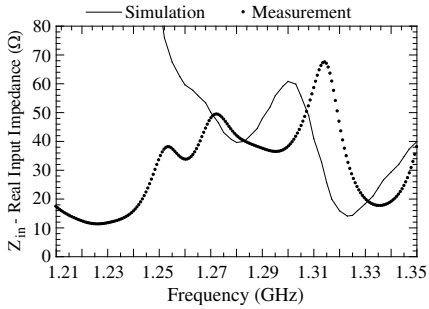

Figure 10. Simulated and measured real input impedance (Z_{in}) plotted as a function of frequency.

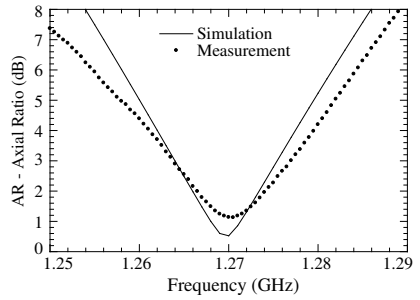

Figure 11. Simulated and measured axial ratio (AR) plotted as a function of frequency.

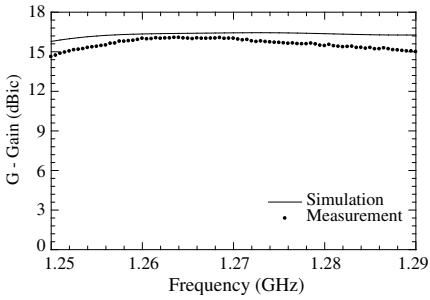

Figure 12. Relationship between antenna gain and frequency at θ angle $= 0^\circ$

In the simulation, on the other hand, the value is 11 MHz, or around 0.87% of the operation frequency. The minimum axial ratio of the measured data is around 1.13 dB, exhibiting a difference of around 0.6 dB as compared with the simulation result. Inaccuracies in the implementation of the corner-truncated patches are one possible cause of differences between the simulated and measured results. This result is mostly acceptable for the satellite-borne CP-SAR antenna, but still insufficient for the UAV-borne antenna with a target specification of 233 MHz (see Table 1). In our future work, more considerations will be needed to further extend the 3-dB AR bandwidth.

In Figure 12, the antenna gain within the CP bandwidth is plotted as a function of frequency. The antenna has a high gain, with the

measured peak gain of about 16.07 dBic at 1.27 GHz. Although this value is slightly lower by around 0.43 dBic as compared with the simulation, the observed value is mostly above the targeted value of 14.32 dBic. Such a difference between the simulated and measured results can probably be ascribed to the slight imperfection in size of patch and feed network offering from milling process, connector, etc.

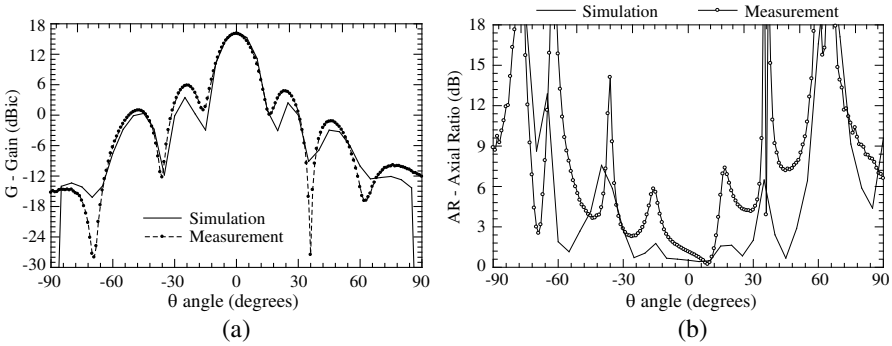

Figure 13. Array antenna characteristics in the theta plane (negative theta for $Az = 180°$ and positive for $Az = 0°$) (x-z plane) at $f = 1.27$ GHz, (a) gain versus theta angle, and (b) axial ratio versus theta angle.

Figure 13 shows the radiation characteristics produced from the array antenna in the theta plane ($Az = 180°$ and $0°$ or Azimuth direction of CP-SAR) at 1.27 GHz. Figure 13(a) shows the distribution of the antenna gain, while Figure 13(b) shows the distribution of the AR. In Figure 13(a), good agreement is seen between the simulated and measured results, both showing that the width of the major lobe exceeding the target gain of 14.3 dBic is around 10°. The first side lobes appear at $\theta = -24°$ with a peak amplitude of 5.85 dB and at $\theta = 23°$ with a peak amplitude of 4.71 dB. Thus, the differences in amplitude between the main and side lobes are around 10.22 and 11.36 dBic for $\theta = -24°$ and 23°, respectively. When the antenna is applied to a platform with altitude higher than 2 km, the side lobe level should be lower than 10 dB of the main beam. Thus, the present result satisfies this requirement. In Figure 13(b), the measured width of the 3-dB AR is 24°, while it is 60° from the simulation. The measured beamwidth is narrower than the simulated result, but still this satisfies the targeted beamwidth of 6.77°.

The antenna characteristics in the theta plane (range direction of CP-SAR) with $Az = 270°$ and 90° are shown in Figure 14. The angular distributions of the gain and AR are plotted in Figures 14(a) and (b),

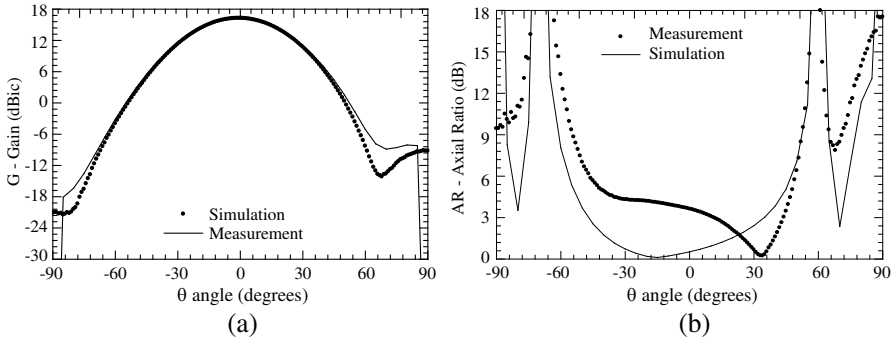

Figure 14. Array antenna characteristics in the theta plane (negative theta for $Az = 270°$ and positive for $Az = 90°$) (y-z plane) at $f = 1.27\,\text{GHz}$, (a) gain vs. theta angle, and (b) axial ratio vs. theta angle.

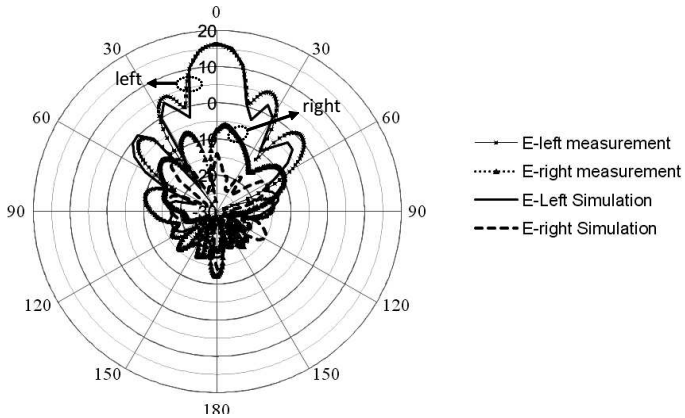

Figure 15. Cross polarization (E-left and E-right pattern) of array antenna at $f = 1.27\,\text{GHz}$.

respectively. In Figure 14(a), similar curves are seen for the simulated and measured results. The beamwidth at 14.3 dBic is around 36°, from −19° to 17°. In Figure 14(b), on the other hand, the measured 3-dB AR beamwidth is around 34°, while the simulation result is 75°. These results indicate that the targeted beamwidth is achieved, satisfying our system requirement.

The cross polarization performance of the array antenna is shown in Figure 15. Based on this graph, the measured peak gain of E-left is about 16.07 dBic at $\theta = 0°$, about 23.53 dBic higher than measured E-right gain value of −7.46 dBic. From this comparison result can

be inferred that the sense of polarization of the array antenna is left-handed circularly polarized (LHCP).

5. CONCLUSION

The characteristics of an L-band circularly-polarized array antenna have been studied for CP-SAR sensor. The method of moment analysis has been used in the simulation study to optimize the antenna design. The performance of a fabricated antenna that produces LHCP has been measured in MRSL. In general, good agreements have been found between the simulated and measured results, indicating that the antenna properties mostly satisfy the target specification as a CP-SAR antenna array. Slight differences between the simulation and measurement are presumably due to imperfections in the manufacturing process including ground plane size, soldering and utilization of connectors, plastic nuts, etc. Based on knowledge on this antenna array, the broadband axial ratio antenna array will be developed in future work, leading to the realization of a CP-SAR antenna onboard UAV and small satellite.

ACKNOWLEDGMENT

The authors would like to thank Merna Baharuddin for the suggestion and sharing; the Japan Society for the Promotion of Science (JSPS) for Grant-in-Aid for Scientific Research 2007-Young Scientist (A) (No. 19686025); National Institute of Information and Communication Technology (NICT) for International Research Collaboration Research Grant; Chiba University COE Start-up Programme "Small Satellite Institute for Earth Diagnosis"; and The Japan Society for The Promotion of Science (JSPS) Japan — East Network of Exchange for Students and Youths (JENESYS) Programme.

REFERENCES

1. Le Vine, D. M., S. D. Jacob, E. P. Dinnat, P. De Matthaeis, and S. Abraham, "The influence of antenna pattern on faraday rotation in remote sensing at L-band," *IEEE Transactions on Geoscience and Remote Sensing*, Vol. 45, No. 9, 2737–2746, 2007.
2. Rignot, E. J. M., "Effect of Faraday rotation on L-band interferometric and polarimetric synthetic-aperture radar data," *IEEE Transactions on Geoscience and Remote Sensing*, Vol. 38, No. 1, 383–390, 2000.

3. Le Vine, D. M. and S. Abraham, "The effect of the ionosphere on remote sensing of sea surface salinity from space: absorption and emission at L band," *IEEE Transactions on Geoscience and Remote Sensing*, Vol. 40, No. 4, April 2002.
4. Maini, A. K. and V. Agrawal, *Satellite Technology: Principles and Applications*, John Wiley, England, 2007.
5. Sri Sumantyo, J. T., H. Wakabayashi, A. Iwasaki, F. Takahashi, H. Ohmae, H. Watanabe, R. Tateishi, F. Nishio, M. Baharuddin, and P. Rizki Akbar, "Development of circularly polarized synthetic aperture radar onboard microsatellite," *PIERS Proceedings*, 382–385, Beijing, China, March 23–27, 2009.
6. Garg, R., P. Bhartia, I. Bahl, and A. Ittipiboon, *Microstrip Antenna Design Handbook*, Artech House, London, 2001.
7. Baharuddin, M., V. Wissan, J. T. Sri Sumantyo, and H. Kuze, "Equilateral triangular microstrip antenna for circularly-polarized synthetic aperture radar," *Progress In Electromagnetics Research C*, Vol. 8, 107–120, 2009.
8. Baharuddin, M., V. Wissan, J. T. Sri Sumantyo, and H. Kuze, "Development of an elliptical annular ring microstrip antenna with sine wave periphery," *Progress In Electromagnetics Research C*, Vol. 12, 27–36, 2010.
9. Baharuddin, M., V. Wissan, J. T. Sri Sumantyo, and H. Kuze, "Elliptical microstrip antenna for circularly-polarized synthetic aperture radar," *International Journal of Electronics and Communications (AEU)*, Vol. 65, No. 1, 62–67, 2010.
10. Rahim, M. K. A., T. Masri, O. Ayop, and H. A. Majid, "Circular polarization array antenna," *Asia-Pacific Microwave Conference*, 1–4, Hong Kong, December 2008.
11. Pozar, D. M. and B. Kaufman, "Increasing the bandwidth of a microstrip antenna by proximity coupling," *Electronics Letters*, Vol. 23, No. 8, 368–369, April 1987.
12. Rizki Akbar, P., J. T. Sri Sumantyo, and H. Kuze, "CP-SAR UAV development," *International Archives of the Photogrammetry, Remote Sensing and Spatial Information Science*, Vol. XXXVIII, Part 8, 203–208, Kyoto, Japan, 2010.
13. Rizki Akbar, P., J. T. Sri Sumantyo, and H. Kuze, "A novel circularly polarized synthetic aperture radar (CP-SAR) onboard spaceborne platform," *International Journal of Remote Sensing*, Vol. 31, No. 4, 1053–1060, 2010.
14. Chen, Z. N. and M. Y. W. Chia, *Broadband Planar Antennas: Design and Applications*, John Wiley & Sons, England, 2006.

15. Hammerstad, E. O., "Equations for microstrip circuit design," *5th European Microwave Conference*, 268–272, Hamburg, Germany, 1975.
16. Abouzahra, M. D. and K. C. Gupta, "Multiport power divider-combiner circuits using circular-sector-shaped planar components," *IEEE Transactions on Microwave Theory and Techniques*, Vol. 36, No. 12, 1747–1752, December 1988.